Graphene electrode platform for impedimetric aptasensing

Yara Aceta[a], Manel del Valle[*]

Sensors and Biosensors Group, Department of Chemistry, Universitat Autònoma de Barcelona, Edifici Cn, 08193 Bellaterra, Barcelona, Spain

Abstract

In this study, we synthesized graphene oxide (GO) at different oxidation times (30, 60 and 120 minutes) using a modified Hummer's method and investigated their carbon-to-oxygen (C/O) ratios, the % C-C double bond, the diffraction pattern, their topography and their electrochemical behaviour both by cyclic voltammetry (CV) and electrochemical impedance spectroscopy (EIS). All GOs synthesized were compared with a GO from commercial source. The graphite-epoxy composite (GEC) electrodes fabricated in our laboratory were modified with GO and electrochemically reduced graphene oxide (ERGO) in preliminary assays to elucidate its applicability for enhanced DNA aptamer biosensing applications.

Keywords:

Graphene oxide; electrochemically reduced graphene oxide; impedance; biosensing; aptasensor; thrombin

[*] Corresponding author: e-mail: manel.delvalle@uab.cat; tel: +34 93 5813235; fax: +34 93 5812379.
[a] Current address: MaCSE Group, Institut des Sciences Chimiques de Rennes, UMR CNRS 6226, Rennes, 35042 France

1. Introduction

Graphite is the most common and thermodynamically stable form of carbon. Its structure has been well documented and consists of an ordered stacking of numerous graphene layers on top of each other [1]. Graphene oxide (GO), normally generated from graphite oxide (GPO), is the product of chemical oxidation and exfoliation of graphite powders. GPO was first synthesized over a century ago [2, 3]. This old material and its by-products have triggered an explosive growth of interest across many disciplines owing to its specific 2D structure and its electrochemical properties [4, 5].

GO, the individual sheets of GPO, is rich in oxygen functional groups and structural defects. These groups (hydroxyl, epoxy, carbonyl and carboxyl) present in the structure of GO offer a wide range of applications by functionalization with various species involving biomolecules such as DNA, RNA and aptamers which are able to interact with GO through carboxyl-to-amine cross-linking (e.g. EDC/NHS amide formation) reaction or via non-covalent bonding (mainly π-π stacking, hydrogen bonds and electrostatic interactions) [6, 7]. Its large specific surface area, biocompatibility, low cost and versatility make GO an advisable material for biosensing applications [8–10], or others, for example, separations [11].

Among other fields, biosensors are widespread in biomedical diagnosis, environmental monitoring, food control and drug analysis. Electrochemical techniques, and mainly sensors based on electrochemical impedance spectroscopy (EIS), are being increasingly used in devices because of the possibility of miniaturization, easy monitoring and carrying out label-free assays [12,13]. Their coupling with

nanomaterials and high-affinity biomolecules allow the highly sensitive and selective detection of a range of analytes [14,15].

Graphene platforms have been used to construct sensitive DNA genosensors by different approaches [13,16]. By using a hairpin DNA conformation, which adsorbs on the graphene layer, it was possible to detect gene sequences correlated to Alzheimer's disease in a variant displaying the decrease of measured impedance [17]; when the DNA probe was attached (via covalent bond) to the graphene layer through one end, the increase of impedimetric signal was then observed [18].

Aptasensors are DNA biosensors which employ aptamers as bio-recognition elements. These are small single stranded DNA or RNA molecules which are obtained by in vitro selection from libraries of synthetic oligonucleotides. Aptamers are able to recognize their respective target molecules with high affinity and specificity; especially, aptamers constitute an interesting alternative to antibodies owing to their easy isolation, long-term stability and wide applicability [19,20].

Well reacted samples of GPO have a carbon to oxygen atomic ratio lying between 2.1 and 2.9 [21]. GPO (or GO) is electrically insulating and thus it cannot be used, without further processing, as a conductive nanomaterial in electrodes [22]. By applying a cathodic potential it is possible to reduce a portion of oxygen functional groups, improving conductivity, but the process cannot restore the sp^2 structure, responsible of the highest electron transfer rate, damaged during the chemical oxidation of graphite [23-26].

Variations in the degree of oxidation of GPO samples are mainly due to the differences between the graphitic sources (size and impurities) and the oxidation protocols followed (oxidation time, reagents and temperature) [22,27]. After applying

the permanganate oxidation route (Hummers' method) [21], a purification protocol needs to be done for eliminating salt impurities, mainly permanganate, sulphate and nitrate anions that remain in solution. It is known that impurities may negatively affect the physical, chemical and electrochemical properties of the nanomaterial [28]. Hummers' purification is based on the treatment of the yellow-brown resulting oxidizing material with cation and anion resin exchangers [21]. Herein we have recovered and adapted this protocol and checked its effectiveness by spectroscopy and elemental analysis. Further functionalization of graphene can be the way to stabilize its suspensions, preventing restacking of grapheme sheets. Recent studies have shown that electrochemical properties in terms of the capacitance of the resulting materials are highly dependent on the graphene preparation method [29].

In this work, therefore, we synthesized GO at different oxidation times (30, 60 and 120 minutes) using the modified Hummers' method and investigated in detail their carbon-to-oxygen (C/O) ratios and the oxygen-containing functional group distribution by X-ray photoelectron spectroscopy (XPS), the diffraction pattern by X-ray powder diffraction (XRD) and their electrochemical behaviour both by CV and EIS. The topography of GO sheets was inspected by transmission electron microscopy (TEM). All GOs synthesized were compared with a GO commercial sample. In order to elucidate the applicability of the GO sheets for designing enhanced DNA biosensors, we performed a preliminary label-free impedimetric assay for detecting thrombin, an important protein mediating in blood coagulation. In this context, the highly sensitive graphite-epoxy composite (GEC) electrodes, usually used in our laboratory, were modified with GO by simple drop-casting. The specific DNA aptamer for thrombin was immobilized by physical adsorption on the GO - modified GEC electrodes. Nyquist plots were recorded before and after the protein-aptamer biorecognition took place. The

possibility of using electrochemically reduced GO (ERGO) as platform where the DNA oligomers are immobilized was also studied and compared with the results obtained with GO.

2. Experimental

2.1 Synthesis of graphite oxide

GPO was synthesized by top-down approach following the modified Hummers' method previously described by Pumera *et al.* [21, 30]. This protocol was applied varying the oxidation time to 30, 60 and 120 min. Briefly, sulphuric acid (35 mL, 98 %) was initially cooled to 0 °C, with subsequent addition of graphite (1.5 g) and $NaNO_3$ (0.75 g). $KMnO_4$ (4.5 g) was added over a period of 2 h and the resulting mixture was then stirred at room temperature for 4 h. Next, it was heated at 35 °C during 30 min. The procedure was repeated in two additional variants heating at 35 °C during 60 min and 120 min. The oxidation process was completed by adding 75 mL of deionised water. The sample was kept at 70 °C for 15 min. After this, the reaction mixture was diluted with 300 mL of deionised water and treated with H_2O_2 solution (30 %) to reduce the residual permanganate and manganese dioxide to colourless soluble manganese sulphate. All reagents were commercially available, of analytical reagent grade and used without further purification. Graphite ultra pure powder was purchased from Merck, sulphuric acid (98 %), sodium nitrate (99 %), potassium permanganate (99 %) were purchased from Sigma-Aldrich; hydrogen peroxide (30 %) was purchased from Riedel-de Haën (Germany),

2.2 Protocol of purification

We have recovered and adapted the Hummers' purification protocol of graphite oxide [21]. Upon the treatment with peroxide, the resulting yellowish – brown paste was washed three times with 1.5 L of deionised water (3 x 500 mL) and recovered by centrifugation at 4000 rpm. Next, the sample of GPO was sequentially treated with cation (DOWEX 50WX4-100) and anion (A520E) exchange resins to eliminate the remaining salts. Sample and resin were kept in contact for 1 h with vigorous stirring. The resins were recovered using two stainless-steel sieves (50 and 100 μm). A negative reaction for sulphate ions with $Ba(NO_3)_2$ was achieved. The GPO slurry was then centrifuged and dried in a vacuum oven at 60 °C for 48 h before use. Cation-exchange resin DOWEX 50WX4-100 was purchased from Sigma-Aldrich and the anion-exchange resin A520E from Purolite. GPO commercial sample was purchased from Nanoinnova Tech. (Madrid, Spain).

2.3 Preparation of graphene-modified electrodes

GO was immobilized on both glassy carbon (GC) and graphite-epoxy composite (GEC) electrodes surface by physical adsorption. For GC electrodes, 20 μL of GO suspension was casted on each electrode surface and dried in oven at 40 ºC. Before using, the excess of non-adsorbed GO material was removed by gentle washing with N,N'–dimethylformamide (DMF). Graphene oxide (GO) was obtained via ultrasonication of 1 mg mL^{-1} dispersion of GPO in DMF for 15 min. DMF (analytical grade) was purchased from Panreac. For the GEC electrodes the same protocol was followed, but in this case, 40 μL of GO at a concentration of 1 mg mL^{-1} in ultra pure water was casted on each electrode surface. ERGO-modified GEC electrodes were achieved by electrochemical reduction of GO previously deposited on a GEC electrode.

2.4 Aptamer immobilization and thrombin incubation

Thrombin aptamer (AptThr) was immobilized on a GO-modified GEC electrode (and on an ERGO-modified GEC electrode) by dry adsorption [31]. 40 μL of a PBS buffer solution with 1 pmol μL^{-1} of AptThr was deposited on each GO-modified GEC electrode and dried at 40 ºC in an oven. Next, the electrodes were washed twice in a PBS buffer solution at room temperature with gentle stirring (250 rpm) to remove the non-adsorbed biomolecule. After that, each AptThr-GO-modified GEC electrode was incubated in an Eppendorf tube with 160μL of a Tris buffer solution containing 5 pM of thrombin at 37 ºC during 30 min with stirring (600 rpm). Resulting electrodes were washed twice in Tris buffer solution at 37ºC before measuring. Buffer solutions employed were: 0.05 M PBS (0.05 M sodium phosphate buffer, pH 7.4); Tris buffer solution consisted in 0.025M Tris + 0.3M NaCl, pH 8.2. The thrombin aptamer (AptThr) used in this study was prepared by TIB-MOLBIOL (Germany) and the target protein thrombin was purchased from Sigma (USA). The AptThr sequence employed was: 5'-TTTGGGTTGGTGTGGTTGG-3'. Stock solutions of aptamer and thrombin were diluted with sterilized and deionised water, separated in fractions and stored at a temperature of − 20 °C. When required, a single fraction was defrosted and used.

2.5 Electrochemical characterization

GO was completely electrochemically reduced on the surface of GC and GEC electrodes by cyclic voltammetry (CV) during 15 cycles in a range of potential from +1.90 V to -2.30 V at 0.1 V s^{-1}. CV experiments were carried out with a glassy carbon (GC) electrode (Ø=3mm), a Ag/AgCl (0.1 M KCl) reference electrode and a platinum

electrode as counter; all EIS experiments were performed with a GEC electrode (Ø=6mm) as working, a Ag/AgCl (0.1 M KCl) pseudo-reference electrode and a platinum electrode as counter. GEC electrodes were prepared as previously reported [32]. All electrochemical experiments were conducted with an IM6e BAS-Zahner potentiostat (Germany) managed with Thales software. The impedimetric detection of thrombin was carried out between 0.5 MHz and 0.1 Hz at a sinusoidal voltage perturbation of 10 mV amplitude. The experiments were performed at room temperature using a solution of 5 mM $[Fe(CN)_6]^{3-/4-}$ (1:1) as redox probe in Tris buffer solution. Nyquist plots were recorded before and after the aptamer-protein bio-recognition taking place, and plots were fitted according to the Randles circuit to obtain the charge transfer resistance (Rct). Results are shown as ΔRct (ratio of the Rct values obtained) [32].

2.5 Spectroscopic characterization

For acquiring the X-ray photoelectron spectra a SPECS PHOIBOS 150 hemispherical energy analyser was used and the XPS spectra were fitted with CasaXPS software package. X-Ray diffraction analysis was performed using a Cu Ka radiation (λ = 1.5418 Å). Transmission electron microscopy (TEM) images were recorded with a JEOL JEM-2011 microscope.

3. Results and Discussion

3.1 GO characterization

Different reported methods to oxidize graphite (according Staudenmaier, Hofmann, or Hummers and Tour) [21, 22, 33, 34] result in materials with different electrochemical and physical properties. In our work, a modified Hummers' method was employed to synthesize GO. The original protocol was modified in order to get some insight about the influence of the oxidation time on the physic-chemical properties of the nanomaterial. For this, GO at 30, 60 and 120 minutes were obtained and are referred as GO30, GO60 and GO120. All samples were compared with a GO commercial (GOC) sample.

The electrochemical behaviour of all samples was studied by CV. All of them, including the commercial product, showed equivalent I-E plots. (Fig.1.A-B) A quasi-reversible behaviour, typical of GO obtained by the permanganate route, was observed for GO30, G060 and GO120. (Fig.1.A and in supplementary info, Fig.A1) A wide peak appeared in the first cathodic scan around – 2.00 V as resulting of two overlapped signals at – 1.82 V and - 2.23 V, and another one appeared in the cathodic region at - 0.95 V during the second scan. As stated in the literature, the GO obtained via the permanganate route contains a greater proportion of carboxyl groups. These groups give well-developed voltammetric waves in aqueous or nonaqueous solvents, but this is usually due to reduction of protons to hydrogen. In aqueous medium and at intermediate pHs, the hydrogen wave appears at - 1.80 V (vs. Ag/AgCl) and aldehydes are reduced at - 1.00 V (vs. Ag/AgCl) to alcohols [35]. Thus during the first cathodic scan the carboxyl groups were reduced to aldehydes, which were also reduced to oxygen in successive cycles at - 1.00 V. After fifteen scans all the oxygen groups in GO were reduced (Fig.1.C) to obtain highly electrochemically reduced graphene oxide (ERGO). Changes in the oxidation state of the GO were followed by EIS using a negatively charged redox probe, the couple $[Fe(CN)_6]^{3-/4-}$. (Fig.1.D) Nyquist plots were recorded and the charge

transfer resistance (Rct) was calculated for a bare GEC electrode before depositing the GO on the electrode surface (black squares), after depositing the GO (blue circles), and once the electroreduction of the oxygen groups was completed (red rhombus). Rct results were 533 ± 1% Ω, 824 ± 1% Ω and 167 ± 3% Ω, respectively. Carboxyl groups on the edge planes of GO are deprotonated at pH 7.2, and thus the Rct for a GO-modified GEC electrode increases in relation to the value of Rct calculated for a bare GEC electrode. After reducing the oxygen groups by CV, the Rct decreases in relation to the value obtained both for a GO-modified GEC electrode and a bare GEC electrode. This is explained by the absence of negatively charged oxygen groups in the surface which electrostatically repelled the redox probe and thus hindered electron transfer.

XPS was employed to analyze in detail the structure of the synthesized GOs. Figure 2 shows the C-1s XPS spectra and deconvoluted peaks for all of them including the commercial product. In all cases, the C-1s XPS spectra indicated a considerable degree of oxidation with six components that correspond to carbon atoms in different oxidation state (hydroxyl, epoxy, aldehyde, carbonyl and carboxyl groups). The C/O ratios were calculated to evaluate the efficiency of the oxidation process (Fig.A2, supplementary info). Table 1 shows the obtained oxygen-containing functional group distribution and the carbon to oxygen ratios (C/O). Well reacted samples of GO had a C/O atomic ratio lying between 2.1 and 2.9. GO30 shows an oxygen group distribution close to the commercial sample, and a C/O value of 2.1. Regarding the GO60 and GO120, results suggest that an overoxidation of the graphite occurs increasing the percentage of carbonyl and carboxyl moieties in relation to GO30. This fact is according with the I-E plots and the wide wave observed around - 2 V.

Another component, namely, the π-π* (HOMO-LUMO) transition that is characteristic for carbon aromatic compounds was observed mainly in the GO120 in the

highest energy range (on the left on Fig. 2). Table 1 shows that the π-π* contribution increased with the oxidation time. The highest amount of epoxy and hydroxyl groups was found in GO30. These groups are placed in the basal planes of GO generating disruptions in the sp^2-structure of the material [36]. On the contrary, the overoxidation of graphite led to a material mainly constituted by carbonyl and carboxyl groups, which were located in the edge plane of GO and are not able to disrupt the conjugated network of graphitic lattice. Thus GO120 showed the highest contribution of the π-π* transition. However the electrical conductivity does not only derives from the sp^2-structure but also from the crystallinity and the defects in the material.

Effect of oxidation time was also examined by X-Ray diffraction (XRD) of the isolated GPOs. Figure 3 shows the powder diffraction spectra for all synthesized GPOs and for the commercial product. The interplanar distance calculated for GPO30, GPO60, GPO120 and GPOC were 7.97 Å, 8.15 Å, 7.79 Å and 7.60 Å, respectively. These results are in good agreement with the literature [24]. The oxidation process modifies the initial stacked structure of graphite. A blue line marks the position where the graphite peak should appear (2θ = ca. 26.4º and d-spacing 3.38 Å). In all samples the peak corresponding with graphite is not observed thus suggesting the complete oxidation of graphite. Graphite oxidation led to an increase in the interplanar distance from 3.38 to ca. 8 Å because of the inclusion of oxygen functional groups placed in both sides of the GPO sheets. The larger the distance between the interlayers, the easier the nanosheets could be further exfoliated. On the other hand, peak profiles are related with the size of the crystals in the sample. Crystals with precise periodicities over long distances have sharp and clear diffraction peaks. Crystals with defects (such as impurities, dislocations, planar faults, or small precipitates) are less precisely periodic in their atomic arrangements and their diffraction peaks are broadened and distorted [31].

As shown in Fig. 3, the XRD peak of GPO30 is narrow and well-defined. It means this material had high periodicity in their structure or minor structural defects in relation to GPO120, which showed a wider peak and also a shoulder peak in its XRD pattern.

Elemental analysis was also carried out to ensure that no impurities or salts remain after the oxidation of the graphite powder. Table 2 shows that the followed purification protocol, based on the treatment of the oxidized graphite with exchange resins, was highly efficient in the removal of the salts impurities. Very low percentages by weight of S (from the H_2SO_4) and N (from the HNO_3) were found, less than 2 % of S and less than 0.1 % of N.

Table 2 also summarizes the C/O ratios calculated by elemental analysis for graphite ultra pure, all the synthesized GPOs samples and the commercial product. A huge difference between the C/O ratios was found by comparison of the starting material and the oxidized samples [38]. The C/O ratio for graphite was 61 while the C/O ratios for the GPOs were ca. 1. It is clear the oxidation of the graphite took place, although the % O is probably overestimated, given the elemental analysis involves the combustion of the sample with oxygen. Consequently, C/O ratios calculated from elemental analysis data are lower than the ratios observed by XPS.

Transmission electron micrographs of GOs samples are shown in Fig. 4. The sheet of GO30 is slightly wrinkled and crumpled around the edges but shows a mono-layered structure. The most oxidized samples, GO60 and GO120 show more wrinkled sheets. This feature can be attributed to point defects in the carbon lattice that cause wrinkling of the sheets on the nanometer scale [39,40]. Alternatively, the commercial product shows flatter sheets but a few-layered structure. Differences in size between the commercial sample and the synthesized GOs could be attributed to differences in the size of the graphite source used for the synthesis of the GPO.

3.2 GO vs. ERGO: thrombin detection

Herein, we show the utility of GO as transducing platform in biosensing. We utilized GO synthesized at 30 min in a preliminary assay to elucidate its applicability for the aptasensing of thrombin, and compared the results obtained with the highly electrochemically reduced ERGO nanomaterial. The GO30 was chosen because of the more favourable physico-chemical properties observed in the characterization: stable suspensions in water; moderate C/O ratio (2.1) and presence of epoxy, carbonyl and carboxyl groups which provides actives points for a physical immobilization of the DNA strains; narrow peaks in the XRD pattern thus assuring a lower presence of defects in its structure; and finally, a mono-layered structure.

Figure 5 shows the responses obtained by EIS for each step of the analysis. Fig. 5-A and Fig. 5-B correspond with the use of a GO30-modified GEC electrode and an ERGO30-modified GEC electrode, respectively. The analytical protocol for biosensing is shown in the Scheme 1. A bare GEC electrode was modified by drop-casting with GO30 (when necessary the GO30 was electroreduced to ERGO30); after that, the thrombin aptamer was immobilized on the GO30-modified electrode by physical adsorption; finally, the AptThr-GO30-modified GEC electrode was incubated in a solution containing the chosen concentration of protein for its detection. All steps were characterized by EIS obtaining the Rct. Results obtained were according with the literature [41,42]. Using GO30, the Rct value increase after the aptamer immobilization due to electrostatic repulsion between the redox probe ($[Fe(CN)_6]^{3-/4-}$) and the negatively charged backbone of the DNA (Fig.5-A). Once the bio-recognition event between the aptamer and the protein took place, the complex aptamer-protein was released from the electrode surface thus decreasing the Rct in accordance with the

concentration of thrombin. To understand the occurring mechanisms one must recall that when employing physical adsorption, the immobilization of oligonuclotide DNA probes onto nanomaterials exploits the hydrophobic and π-π interactions between nucleic acid probes and the nanomaterials. After the aptamer-protein complex formation, a reduction of the impedimetric signal is related to the partial removal of the immobilized ssDNA probes upon the formation of the complex which has weaker interactions with graphene. A more complete explanation of the involved phenomena can be found in the literature [41]. This process has been also exploited using GO nanoplatelets as labels for electrochemical aptasensing [43]. In our experiments, the ΔRct calculated from three replicas was 120 ± 8 Ω.

If the highly electroreduced form of GO30 was used, no clear physical interaction between the aptamer and the ERGO30-modified GEC electrode surface was observed. Probably because of the totally absence of oxygen groups in the surface, the physical immobilization of the AptThr was not achieved and the subsequent incubation with the protein had no effects in terms of change of the Rct. Impedance signal for the ERGO30-modified GEC electrode before and after aptamer immobilization, and after incubating with the protein showed essentially equivalent charge transfer resistance, 116 Ω, 134 Ω and 129 Ω, respectively (Fig.5-B).

On the basis of these results, it is concluded that the synthesized GO30 is an advisable platform for the aptasensing of thrombin, at the pM level, allowing the high sensitive analysis of thrombin protein, in labeless conditions and with a simple experimental design. Shown sensitivity is ca. 10 times equivalent values found with just GEC electrodes [44]. Alternatively, the highly electroreduced form of GO30 (ERGO30) was unable to interact by physical adsorption with the aptamer because of the absence of oxygen groups. In any case, using different electrochemical techniques such as CV

and chronoamperometry it is possible to achieve a desired C/O ratio, and "adapt" the nanomaterial to the changing requirements in biosensing [45], for example to prepare it for physisorption or for covalent bond modification.

4. Conclusions

In summary, we synthesized GO at different oxidation times (30, 60 and 120 minutes) using a modified Hummers' method and investigated their physical-chemical properties. All GOs were compared with a GO commercial product. We found a similar electrochemical behaviour in all the samples, with three peaks in the cathodic region corresponding with the presence of reducible groups like aldehyde, carbonyl and carboxylic groups. It was observed that applying enough current it is possible to reduce the GOs samples thus removing all the oxygen groups on the electrode surface. By XPS the extent of the oxidation and the distribution of oxygen groups in the samples could be characterized. It was found that the material synthesized at 30 min showed a moderate C/O ratio of 2.1 in comparison with the most oxidized sample (GO120) which showed a C/O ratio of 2.8. It is noticeable that the grade of oxidation of the material increased with the oxidation time, thus GO120 showed the largest amount of carbonyl and carboxylic groups. It was shown that the π-π^* contribution increased with the oxidation time, but no conclusions can be derived about the conductivity of the material that also depend on the defects presents in the nanomaterial. By XRD we concluded that the graphite was well oxidized to graphite oxide because of the increase in the d-distance from 3.4 to ca. 8 Å for all samples. The narrow peak observed for GPO30 by XRD made us assume the low proportion of defects in the graphene lattices. TEM images showed the wrinkled and crumpled sheets of the synthesized GOs samples in

comparison with the commercial product. Graphite-epoxy composite (GEC) electrodes, fabricated in our laboratory, were modified with GO30 and ERGO30 to elucidate its applicability for enhanced DNA biosensing applications. On the basis of the preliminary results for the aptasensing of thrombin, we can conclude that the highly ERGO30 nanomaterial cannot be use in aptasensing, the absence of active points in the surface made impossible the aptamer immobilization by physical adsorption. On the contrary, the wrinkled GO30 is an advisable material as platform in biosensing, allowing high sensitive analysis with a simple and labeless biosensing design.

Acknowledgments

Financial support for this work was provided by the Spanish Ministry of Economy and Innovation, MINECO (Madrid) through project CTQ2013-41577-P. Manel del Valle thanks the support from program ICREA Academia. Thanks are due to Alessandro Contini, Chemistry and Pharmacy Department, University of Sassari (Italy), for the XRD experiments.

References

[1] D.D.L. Chung, Review: Graphite, J. Mater. Sci. 37 (2002) 1475–1489. doi:10.1023/A:1014915307738.

[2] M. Pumera, Graphene-based nanomaterials and their electrochemistry, Chem. Soc. Rev. 39 (2010) 4146–57. doi:10.1039/c002690p.

[3] X. Huang, Z. Yin, S. Wu, X. Qi, Q. He, Q. Zhang, Q. Yan, F. Boey, H. Zhang, Graphene-based materials: Synthesis, characterization, properties, and applications, Small 7 (2011) 1876–1902. doi:10.1002/smll.201002009.

[4] A. Ambrosi, A. Bonanni, Z. Sofer, J.S. Cross, M. Pumera, Electrochemistry at chemically modified graphenes, Chem. Eur. J. 17 (2011) 10763–70. doi:10.1002/chem.201101117

[5] M. Pumera, Electrochemistry of graphene, graphene oxide and other graphenoids: Review, Electrochem. Commun. 36 (2013) 14–18. doi:10.1016 /j.elecom.2013.08.028.

[6] T. Kuila, S. Bose, A.K. Mishra, P. Khanra, N.H. Kim, J.H. Lee, Chemical functionalization of graphene and its applications, Prog. Mater. Sci. 57 (2012) 1061–1105. doi:10.1016/j.pmatsci.2012.03.002.

[7] D.R. Dreyer, A.D. Todd, C.W. Bielawski, Harnessing the chemistry of graphene oxide, Chem. Soc. Rev. 43 (2014) 5288–301. doi:10.1039/c4cs00060a.

[8] A.M. Pinto, I.C. Gonçalves, F.D. Magalhães, Graphene-based materials biocompatibility: A review, Colloids Surfaces B Biointerfaces 111 (2013) 188–202. doi:10.1016/j.colsurfb.2013.05.022.

[9] Y. Wang, Z. Li, J. Wang, J. Li, Y. Lin, Graphene and graphene oxide: Biofunctionalization and applications in biotechnology, Trends Biotechnol. 29 (2011) 205–212. doi:10.1016/j.tibtech.2011.01.008.

[10] C. Chung, Y.K. Kim, D. Shin, S.R. Ryoo, B.H. Hong, D.H. Min, Biomedical applications of graphene and graphene oxide, Acc. Chem. Res. 46 (2013) 2211–2224. doi:10.1021/ar300159f.

[11] R.K. Joshi, S. Alwarappan, M. Yoshimura, V. Sahajwalla, Y. Nishina, Graphene oxide: the new membrane material, Appl. Mater. Today,1 (2015) 1-12.

[12] A. Bonanni, M.J. Esplandiu, M. del Valle, Impedimetric genosensors employing COOH-modified carbon nanotube screen-printed electrodes, Biosens. Bioelectron. 24 (2009) 2885–91. doi:10.1016/j.bios.2009.02.023.

[13] A. Bonanni, A. Huiling Loo, M. Pumera, Graphene for impedimetric biosensing, Trends Anal. Chem. 37 (2012) 12-21.

[14] A. Bonanni, M. del Valle, Use of nanomaterials for impedimetric DNA sensors: a review, Anal. Chim. Acta 678 (2010) 7–17. doi:10.1016/j.aca.2010.08.022.

[15] S. Kochmann, T. Hirsch, O.S. Wolfbeis, Graphenes in chemical sensors and biosensors, TrAC Trends Anal. Chem. 39 (2012) 87–113. doi:10.1016/j.trac.2012.06.004.

[16] A. Bonanni, A. Ambrosi, M. Pumera, Nucleic Acid Functionalized Graphene for Biosensing, Chem-Eur. J., 18 (2012) 1668-1673.

[17] A.Bonanni, M.Pumera, Graphene platform for Hairpin DNA based impedimetric genosensing, ACS Nano 5 (2011) 2356-2361.

[18] M. Giovanni, A. Bonanni, M. Pumera, Detection of DNA hybridization on chemically modified graphene platforms, Analyst 137 (2012) 580-583.

[19] J. Ping, Y. Zhou, Y. Wu, V. Papper, S. Boujday, R.S. Marks, T.W.J. Steele, Recent advances in aptasensors based on graphene and graphene-like nanomaterials, Biosens. Bioelectron. 64 (2015) 373–385.

[20] N. de-los-Santos-Álvarez, M.J. Lobo-Castañón, A.J. Miranda-Ordieres, P. Tuñón-Blanco, Aptamers as recognition elements for label-free analytical devices, TrAC - Trends Anal. Chem. 27 (2008) 437–446. doi:10.1016/j.trac.2008.03.003.

[21] W.S. Hummers, R.E. Offeman, Preparation of Graphitic Oxide, J. Am. Chem. Soc. 80 (1958) 1339–1339.

[22] D.C. Marcano, D. V Kosynkin, J.M. Berlin, A. Sinitskii, Z. Sun, A. Slesarev, L.B. Alemany, W. Lu, J.M. Tour, Improved synthesis of graphene oxide, ACS Nano 4 (2010) 4806–14. doi:10.1021/nn1006368.

[23] E. Casero, a. M. Parra-Alfambra, M.D. Petit-Domínguez, F. Pariente, E. Lorenzo, C. Alonso, Differentiation between graphene oxide and reduced graphene by electrochemical impedance spectroscopy (EIS), Electrochem. Commun. 20 (2012) 63–66. doi:10.1016/j.elecom.2012.04.002.

[24] O.C. Compton, B. Jain, D. A. Dikin, A. Abouimrane, K. Amine, S.T. Nguyen, Chemically active reduced graphene oxide with tunable C/O ratios, ACS Nano 5 (2011) 4380–91. doi:10.1021/nn1030725.

[25] S. V. Tkachev, E.Y. Buslaeva, A. V. Naumkin, S.L. Kotova, I. V. Laure, S.P. Gubin, Reduced graphene oxide, Inorg. Mater. 48 (2012) 796–802. doi:10.1134/S0020168512080158.

[26] M.A. Ali, K. Kamil Reza, S. Srivastava, V.V. Agrawal, R. John, B.D. Malhotra, Lipid-lipid interactions in aminated reduced graphene oxide interface for biosensing application, Langmuir 30 (2014) 4192–201. doi:10.1021/la4049852.

[27] D.-W. Kang, H.-S. Shin, Control of size and physical properties of graphene oxide by changing the oxidation temperature, Carbon Lett. 13 (2012) 39–43. doi:10.5714/CL.2012.13.1.039.

[28] V. Singh, D. Joung, L. Zhai, S. Das, S.I. Khondaker, S. Seal, Graphene based materials: Past, present and future, Prog. Mater. Sci. 56 (2011) 1178–1271. doi:10.1016/j.pmatsci.2011.03.003.

[29] A. Bonanni, M. Pumera, High-resolution impedance spectroscopy for graphene characterization, Electrochem. Commun. 26 (2013) 52-54.

[30] A.Y.S. Eng, A. Ambrosi, C.K. Chua, F. Saněk, Z. Sofer, M. Pumera, Unusual inherent electrochemistry of graphene oxides prepared using permanganate oxidants, Chem. Eur. J. 19 (2013) 12673–83. doi:10.1002/chem.201301889.

[31] A. Bonanni, I. Fernández-Cuesta, X. Borrisé, F. Pérez-Murano, S. Alegret, M. del Valle, DNA hybridization detection by electrochemical impedance spectroscopy using interdigitated gold nanoelectrodes, Microchim. Acta 170 (2010) 275–281. doi:10.1007/s00604-010-0358-5.

[32] C. Ocaña, C. Figueras, M. del Valle, Avidin Epoxy-Graphite Composite Electrodes as Platforms for Genosensing and Aptasensing, J. Nanosci. Nanotechnol. 14 (2014) 6669–6677. doi:10.1166/jnn.2014.9357.

[33] L. Staudenmaier, Verfahren zur Darstellung der Graphitsäure, Berichte Dtsch. Chem. Gesellschaft 31 (1898) 1481–1487. doi:10.1002/cber.18980310237.

[34] U. Hofmann, E. Konig, Untersuchungen uber Graphitoxyd, Z. Anorg. Allg. Chem. 234 (1937) 311–336. doi:10.1002/zaac.19372340405.

[35] O. Hammerich, B. Speiser (Eds.), Organic Electrochemistry. Revised and Expanded, 5th Edn, CRC Press, Boca Raton FL, 2015.

[36] G. Kucinskis, G. Bajars, J. Kleperis, Graphene in lithium ion battery cathode materials: A review, J. Power Sources 240 (2013) 66–79.

[37] B. Fultz, J. Howe, Diffraction and the X-Ray Powder Diffractometer, in: Transmission Electron Microscopy and Diffractometry of Materials, Springer, Berlin, 2013: pp. 1–57. doi:10.1007/978-3-642-29761-8_1.

[38] A. Ambrosi, C.K. Chua, A. Bonanni, M. Pumera, Lithium Aluminum Hydride as Reducing Agent for Chemically Reduced Graphene Oxides, Chem. Mater. 24 (2012) 2292–2298. doi:10.1021/cm300382b.

[39] C. Gomez-Navarro, Electronic transport properties of individual chemically reduced graphene oxide sheets, Nano Lett. 7 (2007) 3499–3503. doi:10.1021/nl072090c.

[40] H.C. Schniepp, J.-L. Li, M.J. McAllister, H. Sai, M. Herrera-Alonso, D.H. Adamson, R.K. Prud'homme, R. Car, D. A. Saville, I. A. Aksay, Functionalized single graphene sheets derived from splitting graphite oxide, J. Phys. Chem. B. 110 (2006) 8535–9. doi:10.1021/jp060936f.

[41] A.H. Loo, A. Bonanni, M. Pumera, Biorecognition on graphene: Physical, covalent, and affinity immobilization methods exhibiting dramatic differences, Chem. - An Asian J. 8 (2013) 198–203. doi:10.1002/asia.201200756.

[42] A. Ambrosi, C.K. Chua, A. Bonanni, M. Pumera, Electrochemistry of graphene and related materials, Chem. Rev. 114 (2014) 7150–88. doi:10.1021/cr500023c.

[43] A.H. Loo, A. Bonanni, M. Pumera, Thrombin aptasensing with inherently electroactive graphene oxide nanoplatelets as labels, Nanoscale 5 (2013) 4758-4762. doi: 10.1039/c3nr00511a

[44] C. Ocaña, M. Pacios, M. del Valle, A Reusable Impedimetric Aptasensor for Detection of Thrombin Employing a Graphite-Epoxy Composite Electrode, Sensors 12 (2012) 3037-3048. doi:10.3390/s120303037

[45] A. Ambrosi, M. Pumera, Precise tuning of surface composition and electron-transfer properties of graphene oxide films through electroreduction, Chem. Eur. J. 19 (2013) 4748–53. doi:10.1002/chem.201204226.

Table 1. Tabulated carbon/oxygen ratios from the X-ray photoelectron spectra of the studied graphene forms GO30, GO60, GO120, and GOC, and quantitative distributions of deconvoluted peaks from their high-resolution C-1s spectra.

C-1s peak	Binding energy (eV)	GO30 (%)	GO60 (%)	GO120 (%)	GOC (%)
C=C	284.3	30.3	20.5	14.6	34.5
C-C	285.0	12.3	12.0	15.0	8.6
C-O	286.4	38.0	35.5	20.3	41.6
C=O	287.2	11.2	14.6	21.4	9.6
O-C=O	288.3	6.5	13.5	17.5	5.7
$\pi - \pi^*$	292.4	1.6	4.0	11.2	-
C/O		2.1	2.1	2.8	1.8

Table 2. Elemental analysis of graphite and graphene oxide obtained at different oxidation times: 30 min (GPO30), 60 min (GPO60), 120 min (GPO120); comparison against the commercial samples (GOC).

	% by weight				
Sample	% C	% O	% S	% N	C/O
Graphite	98	1.6	<0.1	<0.1	61.3
GPO30	48	48	2.0	<0.1	1.0
GPO60	44	52	1.2	<0.1	0.9
GPO120	51	46	1.2	<0.1	1.1
GOC	51	47	0.9	<0.1	1.1

FIGURE CAPTIONS

Figure 1. I-E plots of GO synthesized by top down approach at 30 min (A) and a GO of commercial source (B) on a GC electrode in 0.05 M PBS + 0.1 M KCl; (C) Multiple-cycle anodic voltammograms of GO30 on a GEC electrode in 0.05 M PBS + 0.1 M KCl. (D) Impedimetric characterization of the different forms of obtained graphene, GO and ERGO, deposited on a GEC electrode; measures in 0.05 M PBS + 0.1 M KCl containing 5 mM of $[Fe(CN)_6]^{3-/4-}$(1:1) as redox probe..

Figure 2. C-1s XPS spectra and deconvoluted peaks recorded for the GO obtained at different reaction times. (A) GO obtained after reaction time of 30 min. (B) GO obtained after reaction time of 60 min. (C) GO obtained after reaction time of 120 min. (D) GO of commercial source. Blue lines corresponding to the fit.

Figure 3. X-Ray powder diffraction patterns of the different GPOs studied in this work. (A) GPO obtained after reaction time of 30 min. (B) The others GPOs assayed: GPO60, GPO obtained after reaction time of 60 min, GPO120, GPO obtained after reaction time of 120 min and GPOC, GO of commercial source.

Figure 4. TEM images of the GO synthesized in our laboratory by modified Hummers' method. (A) GO obtained after reaction time of 30 min. (B) GO obtained after reaction time of 60 min. (C) GO obtained after reaction time of 120 min. (D) GO of commercial source. For each sample the powder was previously suspended in ethanol absolute (≥ 99.8 %) and sonicated during 15 min. After that, a drop of solution was casted on a cupper TEM grid for its observation.

Figure 5. Impedimetric sensing of Thrombin using its DNA aptamer immobilized on graphene-modified GEC electrodes: (A) Use of GO30 modified electrode, before (●) and after the modification with thrombin aptamer (●), and after incubation with a solution of 5 pM thrombin (♦). Conditions: 0.025 M Tris buffer solution + 0.1 M KCl containing 5 mM of $[Fe(CN)_6]^{3-/4-}$(1:1) as redox probe; (B) Use of ERGO modified electrode, before its modification (■), after application of GO-GEC (●), after electrochemical reduction ERGO-GEC (♦), after immobiliation of aptamer AptThr-ERGO-GEC (▲), and after incubation with thrombin ThrAptThr-ERGO-GEC (▼). Conditions: 0.05 M PBS + 0.1 M KCl containing 5 mM of $[Fe(CN)_6]^{3-/4-}$(1:1) as redox probe. Three replicas were done for each experiment.

Scheme 1. Schematic diagram of the protocol followed to immobilize the thrombin aptamer on the GO-GEC electrode and for detecting the thrombin protein. Step 1: a bare GEC electrode is modified by drop-casting with GO30; step 2: dry adsorption of the thrombin aptamer on the GO30-modified GEC electrode surface; step 3: incubation of the AptThr-GO30-modified GEC electrode with the thrombin protein. The bio-recognition event takes place between the aptamer and the protein releasing the complex aptamer-protein from the electrode surface. All steps were characterized by EIS to obtain the Rct.

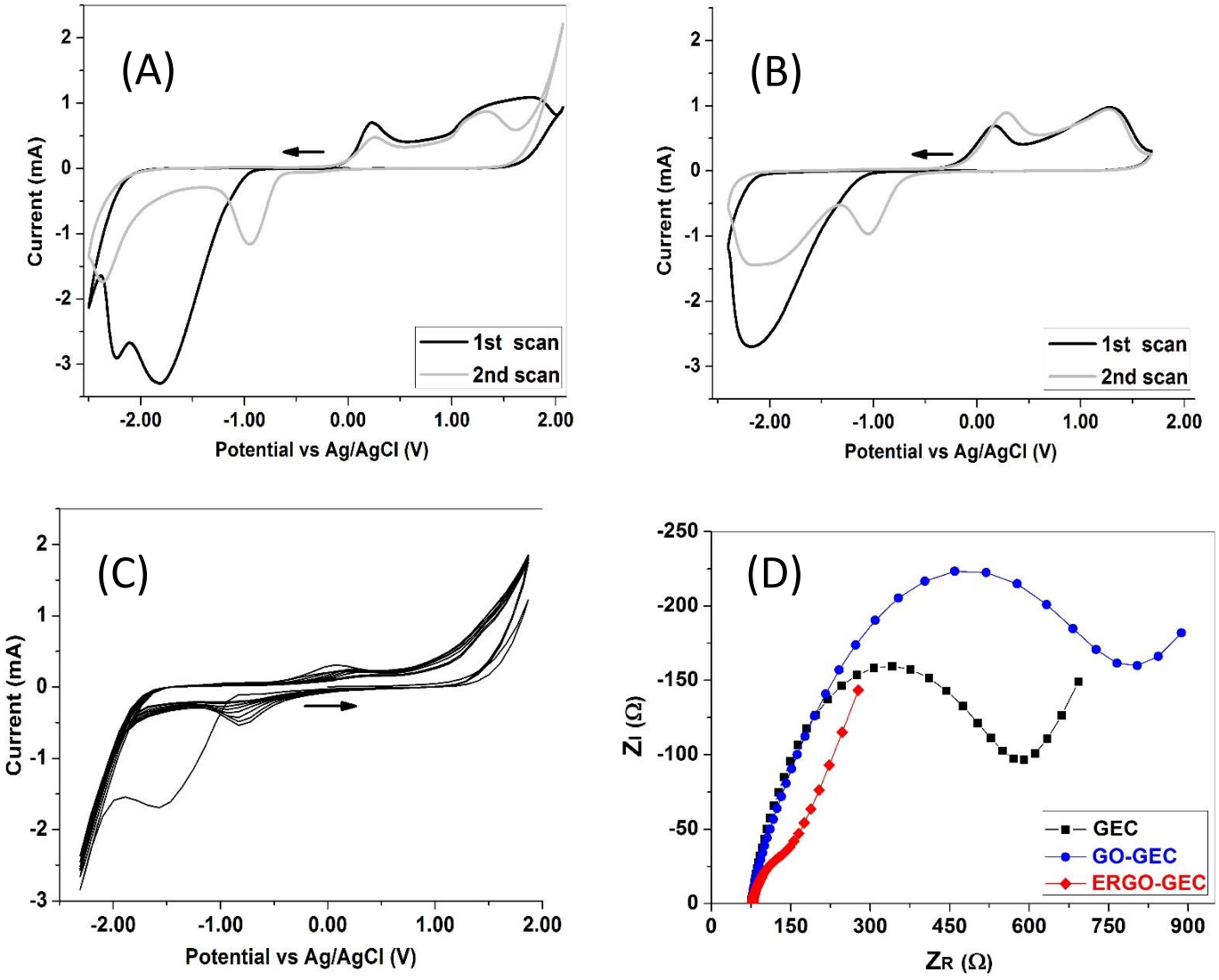
(A)
Current (mA)
Potential vs Ag/AgCl (V)
1st scan
2nd scan
(B)
Current (mA)
Potential vs Ag/AgCl (V)
1st scan
2nd scan
(C)
Current (mA)
Potential vs Ag/AgCl (V)
(D)
ZI (Ω)
ZR (Ω)
GEC
GO-GEC
ERGO-GEC

Figure 1

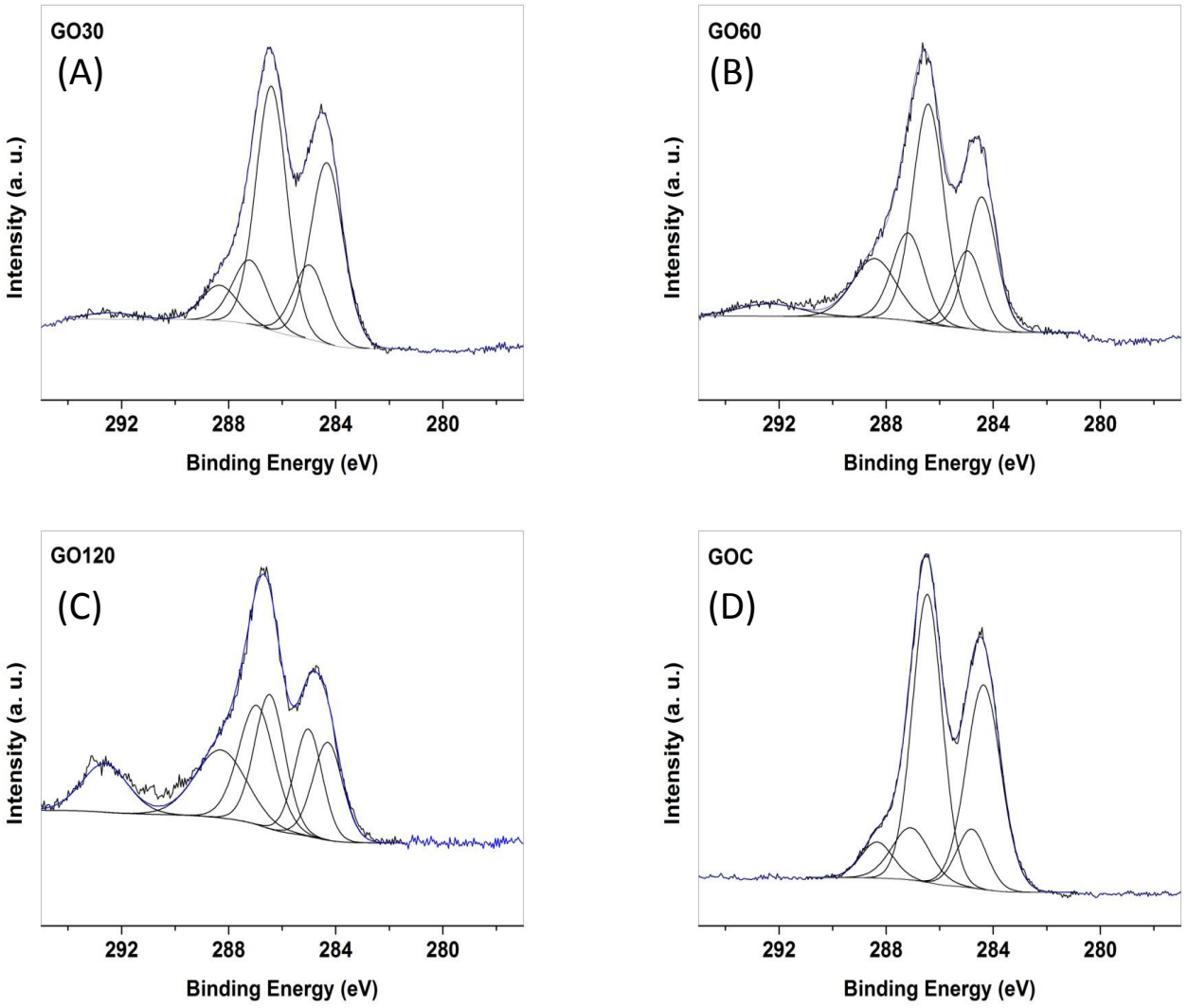
GO30
(A)
Intensity (a. u.)
292
288
284
280
Binding Energy (eV)
GO60
(B)
Intensity (a. u.)
292
288
284
280
Binding Energy (eV)
GO120
(C)
Intensity (a. u.)
292
288
284
280
Binding Energy (eV)
GOC
(D)
Intensity (a. u.)
292
288
284
280
Binding Energy (eV)

Figure 2

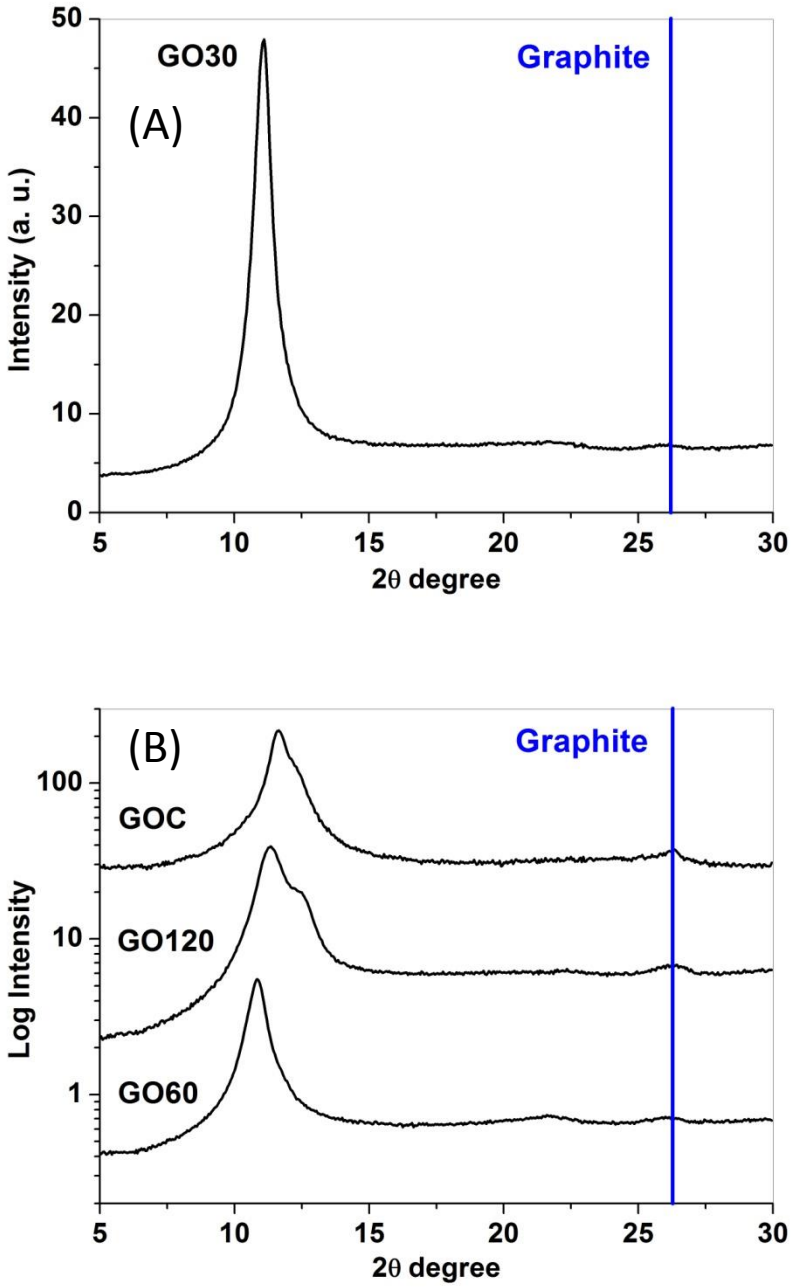
GO30
Graphite
(A)
Intensity (a. u.)
50
40
30
20
10
0
5
10
15
20
25
30
2θ degree
(B)
Graphite
GOC
GO120
GO60
Log Intensity
100
10
1
5
10
15
20
25
30
2θ degree

Figure 3

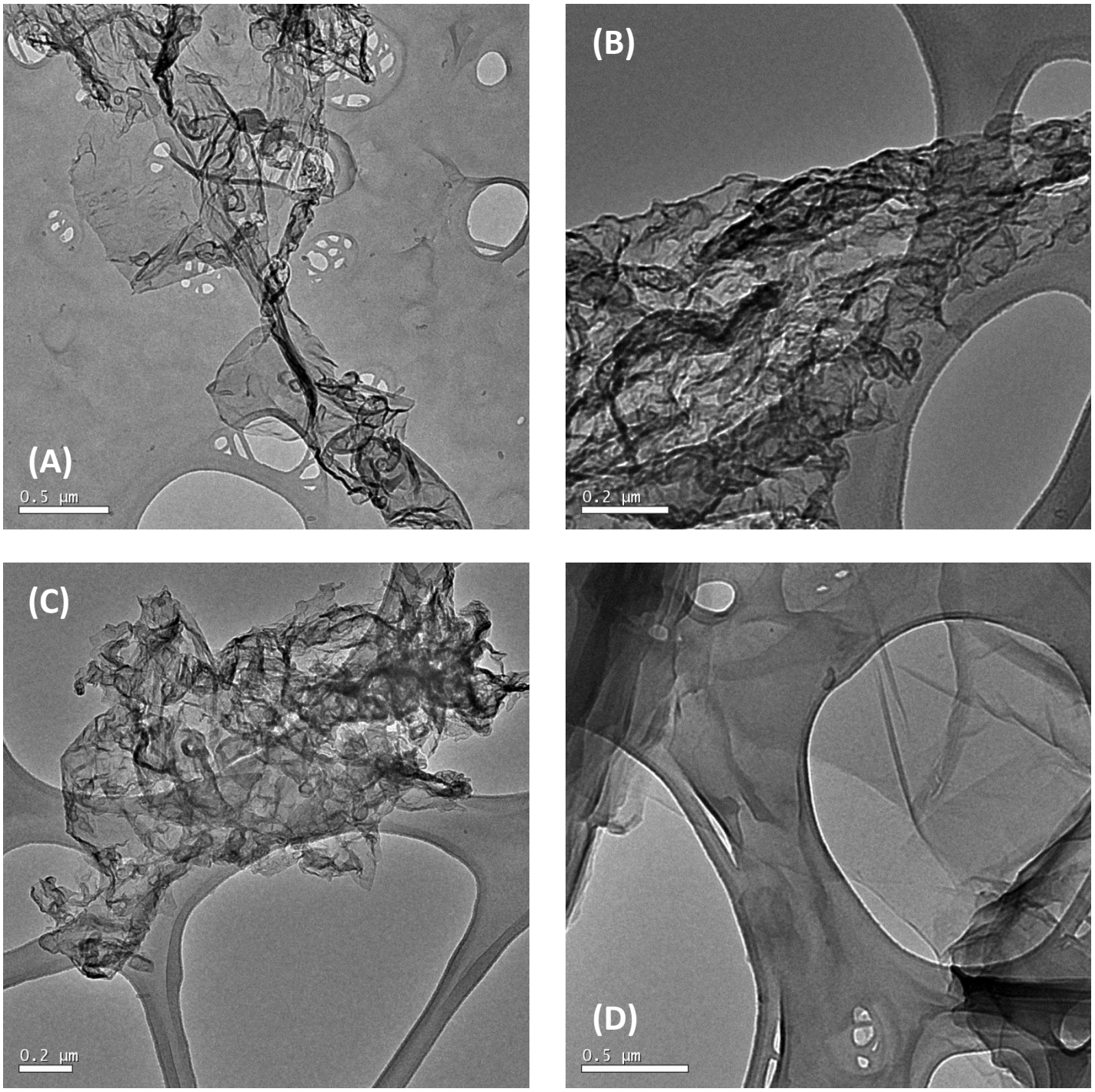

Figure 4

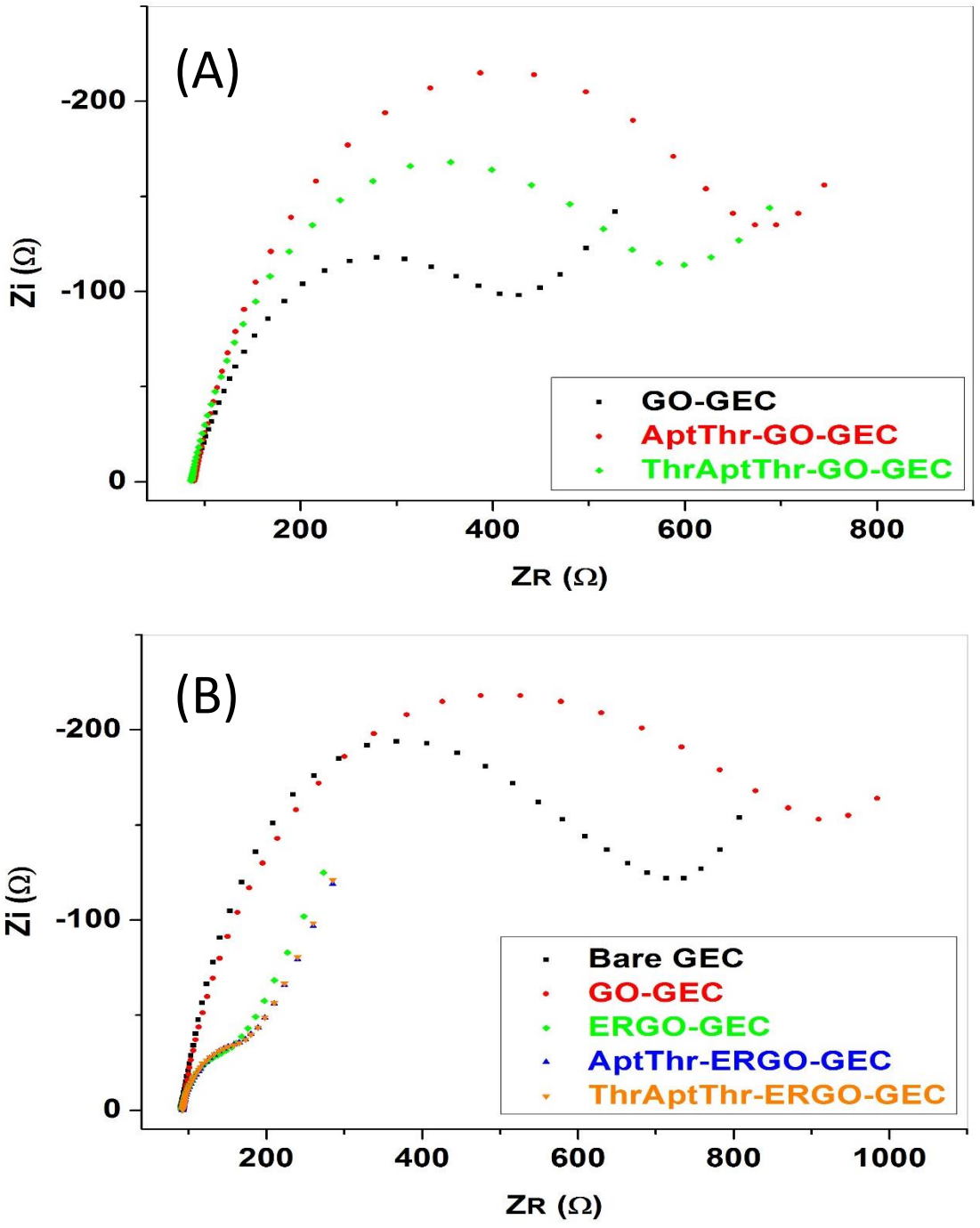
(A)
-200
-100
0
Zi (Ω)
200
400
600
800
ZR (Ω)
GO-GEC
AptThr-GO-GEC
ThrAptThr-GO-GEC
(B)
-200
-100
0
Zi (Ω)
200
400
600
800
1000
ZR (Ω)
Bare GEC
GO-GEC
ERGO-GEC
AptThr-ERGO-GEC
ThrAptThr-ERGO-GEC

Figure 5

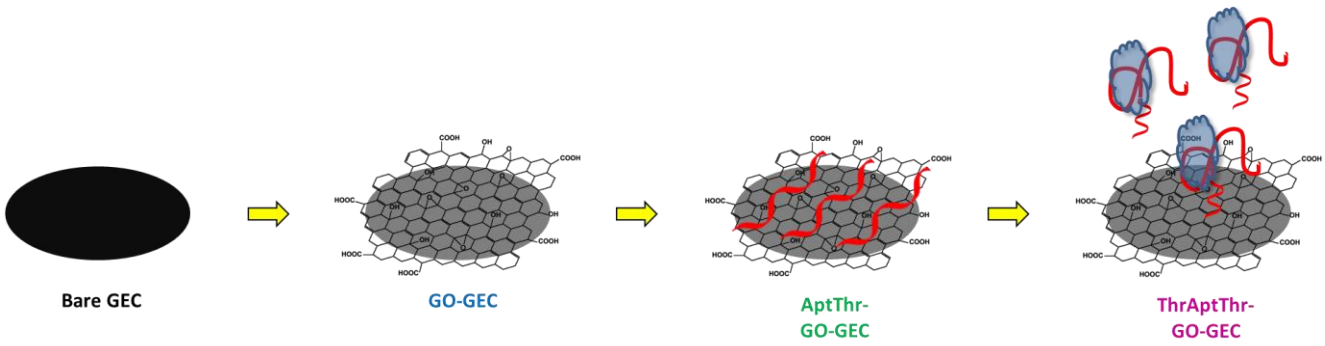

Scheme 1